

3D volumes constructed from pixel-based images by digitally clearing plant and animal tissue

D.P. LIVINGSTON, III*, T.D. TUONG*, S.R.V. GADI†,
C.H. HAIGLER‡, R.S. GELMAN§ & J.M. CULLEN†

*USDA and North Carolina State University, Raleigh, North Carolina, U.S.A.

†College of Veterinary Medicine, North Carolina State University, Raleigh, North Carolina, U.S.A.

‡North Carolina State University, Raleigh, North Carolina, U.S.A.

§BeltlineMedia, Norwalk, Connecticut, U.S.A.

Key words. Adobe After Effects, biopsy, frozen plant, *in situ* hybridization, light microscopy, liver, lung, paraffin, radiofrequency ablation, tumour, 3D reconstruction.

Summary

Construction of three-dimensional volumes from a series of two-dimensional images has been restricted by the limited capacity to decrease the opacity of tissue. The use of commercial software that allows colour-keying and manipulation of two-dimensional images in true three-dimensional space allowed us to construct three-dimensional volumes from pixel-based images of stained plant and animal tissue without generating vector information. We present three-dimensional volumes of (1) the crown of an oat plant showing internal responses to a freezing treatment, (2) a sample of a hepatocellular carcinoma from a woodchuck liver that had been heat-treated with computer-guided radiofrequency ablation to induce necrosis in the central portion of the tumour, and (3) several features of a sample of mouse lung. The technique is well suited to images from large sections (greater than 1 mm) generated from paraffin-embedded tissues. It is widely applicable, having potential to recover three-dimensional information at virtually any resolution inherent in images generated by light microscopy, computer tomography, magnetic resonance imaging or electron microscopy.

Introduction

Current 3D reconstruction technology

The ability to view internal structures in three dimensions (3D) has aided the medical community in the diagnosis of a variety

of detrimental conditions. Magnetic resonance imaging (MRI) and positron emission tomography/computed tomography (PET/CT) have been used to generate 3D volumetric image reconstructions using a technique called '3D-maximum intensity reconstruction' of a fused data set (Badea *et al.*, 2008). These reconstructions provide invaluable information about numerous normal conditions, such as heart and brain function, as well as pathologies such as the presence and/or the spread of cancer. The use of MRI and CT technologies among researchers in other disciplines has been restricted because of cost as well as limits in resolution (10 µm for MRI, Ferrando & Spiess, 2000). Synchrotron radiation imaging (SRI) produces images at considerably better resolution (Peyrin, 2009), but it is not widely used because of its expense and the limited number of facilities worldwide. These factors prevent the use of CT, MRI and SRI in routine observations of small structures such as plant tissues or biopsies.

Confocal laser scanning microscopy (CLSC) has been used for 3D localization of various fluorescing compounds within biological tissues at higher resolution than MRI or CT (see Ferrando & Spiess, 2000; Hepler & Gunning, 1998, for reviews). A limitation of CLSC, however, is that tissue penetration typically cannot exceed 0.2–0.35 mm and subcellular features are most commonly analysed through relatively high magnification objective lenses (Sauermann *et al.*, 2002; Kaeb & Landthaler, 2009). Therefore, only small pieces of plant or animal tissue can be imaged at one time. Despite this limitation, numerous important discoveries in both plant and animal tissue have been made using CLSC (Shotton, 1989; Hepler & Gunning, 1998; Hutzler *et al.*, 1998; Angeles *et al.*, 2004). A reconstruction method similar to confocal techniques using light microscopy to photograph fossil specimens at varying focal planes and using

Correspondence to: David P. Livingston, USDA and North Carolina State University, 840 Method Road, Unit 3, Raleigh, NC 27695, U.S.A. Tel: +1-919-515-4324; fax: +1-919-515-2305; e-mail: david.livingston@ars.usda.gov

commercially available software to build 3D volumes was described (Haug *et al.*, 2009).

CLSC, MRI and PET/CT allow optical sectioning and are noninvasive therefore, permit observations not only in three spatial dimensions but also in the fourth dimension, time (Badea *et al.*, 2008).

Software used for 3D reconstruction

Software has been developed to produce 3D reconstructions from 2D images of serially sectioned tissue, primarily among researchers using electron microscopy. This has made it possible to generate 3D images almost routinely at nearly any resolution. In brief, serial images are aligned with each other and then contours are drawn around features of interest in each 2D image; the software then generates a 3D model from the vector-based contours.

For example, using the software IVE (Chen *et al.*, 1996) and IMOD (Kremer *et al.*, 1996), nanoparticle transmigration into the liposome was illustrated (Bihan *et al.*, 2009). Mitochondrial transformation during apoptosis was described for the first time using IMOD (Sun *et al.*, 2007). A potassium channel subunit and a water channel aquaporin were localized to the cerebellar pinceau (Bobik *et al.*, 2004) using IMOD and several other suites of software. Of all the 3D, contour-tracing reconstruction software, IMOD is arguably the most common. In addition, some labs have generated their own software to address specific research needs (Kriete & Schwebel, 1996; Marko & Leith, 1996; Bobik *et al.*, 2004).

Limitations of available software

Although noteworthy discoveries have been made from 3D reconstruction using contour-tracing software, depending on the complexity of the tissue and the number of internal features of interest, drawing accurate contours can be tedious. This is particularly true of serial-sections from light microscopy of plant tissue because of considerable branching of stems and roots as well as numerous intertwining vessel elements in some plant organs, as, for example within the crown tissue of winter cereals (Livingston *et al.*, 2005). In addition, modelling only structures around which contours are traced can result in the loss of potentially important details in original images. This may be advantageous if certain details in an image interfere with objects of interest. But, important features could be overlooked if the researcher focused only on the structure(s) around which contours were traced.

Tissue clearing is a major hurdle to 3D reconstruction

Difficulty viewing features of interest within complex tissues often arises from interfering or excessive opacity of surrounding tissue. Even in CLSC limited depth of signal-harvesting arises from interfering opacity of the tissue. One

method of overcoming this difficulty for fixed samples is to make surrounding tissue clear, allowing the researcher to see internal features of interest. Some time ago Zimmerman (1893) described several chemical and physical methods of clearing tissue to allow observation of internal structures of plants, and similar methods continue to be used. Berleth & Jurgens (1993) identified the effect of the monopteros gene on root development in *Arabidopsis* partly by using chloral hydrate to view the internal structure of embryos. Tissue clarification procedures have been described (Liedl *et al.*, 1993; Beekman & Engler, 1994; Lux *et al.*, 2005) and used to view the location of GUS activity and to visualize internal structures of roots in *Arabidopsis*, maize and sorghum. A clearing technique for visualizing cellular structure in animal tissue was described by Harrison & Anderson (1974). A major disadvantage of chemical clearing is that chloral hydrate is a controlled substance, and many intact tissues are too thick to generate high-resolution light micrographs even after chemical clearing.

Digital clearing allows building of 3D volumes

In this paper, we demonstrate a digital method of clarifying biological tissue based on colour-recognition software found within Adobe After Effects (AE) commonly used in the visual effects industry to remove ('key-out') studio back ground colours. Also known as 'chroma-keying' and 'green (or blue)-screen technology', this technique allows a different background to be inserted into a commercial movie scene. We demonstrate that the same technology can be used to make the tissue surrounding regions of scientific interest transparent, thereby allowing the construction of 3D volumes from serial paraffin sections of plant and animal tissues imaged by light microscopy or from stained sections photographed directly with a digital camera.

Materials and methods

Production of serial 2D images from three biological tissues

Frozen oat (Avena sativa) crown (Fig. 1). Seeds of oat (cv. 'Wintok') were planted and grown under controlled conditions as described (Livingston *et al.*, 2005). Eight-week-old plants that had been cold-acclimated were frozen to -12°C for 3 h and then warmed to 2°C (see Livingston *et al.*, 2005 for details). Thawed plants were then allowed to grow for 7 days at 13°C . The bottom 1 cm of the stem, above the roots (crown), was removed and subjected to microwave-assisted fixation, dehydration and paraffin embedding previously described (Livingston *et al.*, 2009). The embedded crown was serially sectioned at $25\ \mu\text{m}$ and stained with Safranin and Fast Green.

Sections were photographed with a digital camera (Sony DSC707) attached to a Nikon Eclipse 50i microscope with a $2\times$ objective and 30 W halogen lamp.

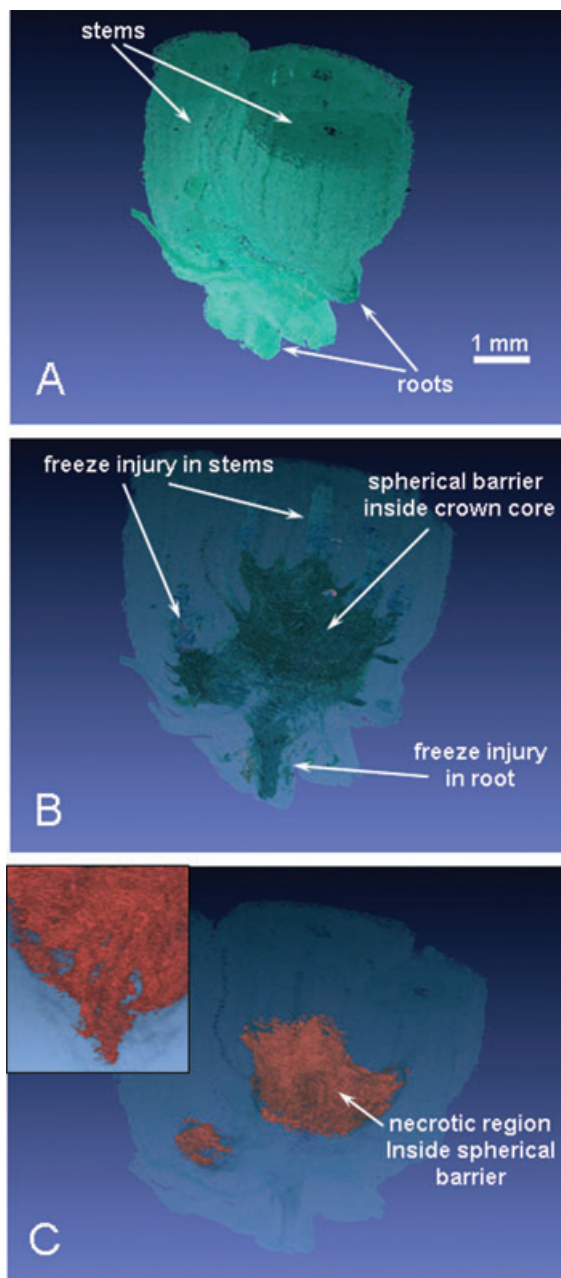


Fig. 1. 3D volume constructed from 180 JPEG images of a frozen oat crown that was allowed to recover from freezing for 7 days. Still images were freeze-frames taken from the supplementary video in D. (A) Outside of the plant with actual colour of the original Safranin/Fast-Green stained images. Note roots at the bottom and stems at the top of the crown. (B) Frozen oat crown with undamaged tissue cleared digitally showing regions of the interior of the crown that stained differently as a result of the freezing treatment. (C) Central portion of the crown on the inside of the barrier (shown in B) in which tissue was significantly disrupted from freezing and is presumed to be necrotic. Note the inset which is a freeze frame from the opposite side of the crown showing several vertical channels of empty space that have been filled with a solid orange colour. (D) *Supplementary video file* with rotation, scaling, clearing and re-colourizing of the tissue in an animated video. See supporting information in the online version of this article.

Woodchuck (Marmota monax) liver (Fig. 2). A hepatocellular carcinoma identified by CT in the liver of a woodchuck was subjected to computer-guided radiofrequency ablation (Curley, 2001; Patriciu *et al.*, 2005). Liver was collected immediately postmortem. Liver tumour and adjacent normal liver tissue were fixed by immersion in 10% neutral buffered formalin and processed using a routine paraffin protocol for sectioning. Liver tissue was serially sectioned at 4 μm and stained with a standard, eosin/haematoxylin (H&E) stain. Slides were placed on a light box and photographed with a digital camera (Sony DSC707) without the use of a microscope.

Mouse (Mus musculus) lung (Fig. 3). During postmortem examination, a mouse trachea and lung was fixed by perfusion with 10% neutral buffered formalin then fixed and embedded in paraffin. A 0.5 cm square block of tissue was cut from a larger sample and re-embedded in paraffin. Serial 10 μm sections were stained with H&E stain and photographed on a Nikon microscope with a 2 \times objective.

Software manipulation of 2D images

Importing and aligning images. Individual JPEG images (180 for the oat crown, 66 for the woodchuck liver and 60 for the mouse lung) were downloaded from the camera to a MacPro computer (2 \times 2.8 Quad-Core Intel Xeon Processor, 12 GB RAM memory) and imported as a sequence into Adobe After Effects version 9.02 (a component of Adobe CS4; Adobe Systems Inc., San Jose, CA). Images were aligned manually by importing all images as footage and using very simple AE alignment tools. After some practice, manual alignment took 1 h to align 60 images and allowed nearly perfect registration of images. Although occasional image distortion due to stretching of paraffin made alignment more difficult, the final 3D image was not significantly affected by minor variances in a few sections. Images that were lost during processing or severely distorted were not included in the final reconstructions.

Digital clearing. Various colour-keying routines under the effects menu (e.g. Keylite, colour key and Luma key) were used to remove the background from all the images in the sequence simultaneously. These same routines were then used to 'key-in' or 'key-out' specific colour values or colour ranges as well as to change the opacity of layers. In monochrome images (not shown), differences in luminance were used to key-out (or key-in) specific tissues. This 'digital clearing' essentially allowed us to look inside the tissue at any object that was stained differentially or was individually masked (see section "Using a mask to select a specific feature") and colour-enhanced. To change the colour uniformly in the image, the colour correction routine in the effects menu called 'tint' was used.

3D volume construction. Once the images were aligned and the background, as well as other unwanted tissue, was

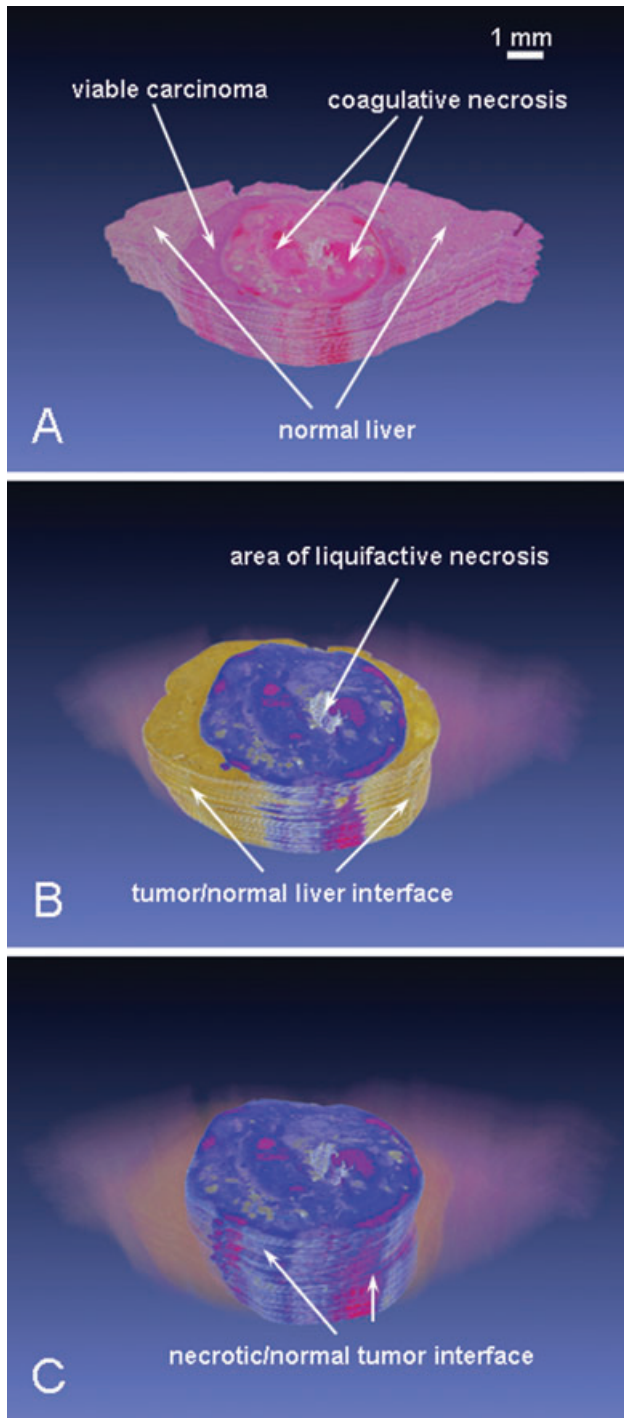


Fig. 2. 3D volume of a sample of liver from a woodchuck constructed from 65 JPEG images. These figures were taken as freeze-frames from the supplemental video in D. (A) Actual colour of all H&E-stained images in a stack. (B) Liver sample in which the surrounding tissue was cleared showing the live (re-colourized to yellow) and necrotic (re-colourized to blue) tumour. (C) Portion of liver in which noncancerous tissue and live tumour were cleared showing only the necrotic, heat-treated portion of the tumour. (D) *Supplemental video file* with rotation, scaling, clearing and re-colourizing of the tissue in an animated video. See supporting information in the online version of this article.

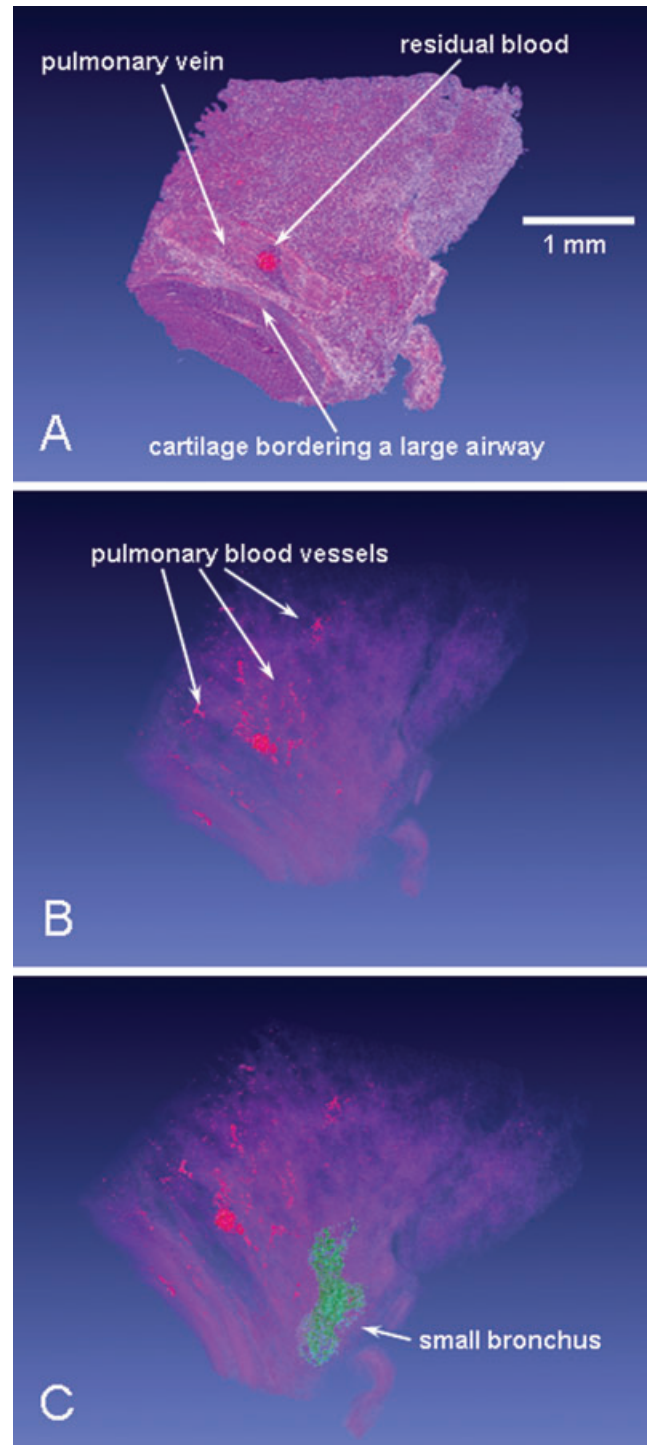


Fig. 3. 3D volume of normal lung tissue from a mouse constructed from 60 JPEG images. Still images were freeze-frames taken from the supplemental video in D. (A) Actual colour of all H&E-stained images in a stack. (B) Mouse lung with surrounding tissue cleared showing pulmonary blood vessels within the tissue. (C) Most of the lung cleared showing a small bronchus re-colourized to green. The 3D structure of the bronchus is evident in the Supporting Information in D. (D) *Supplemental video file* with rotation, scaling, clearing and re-colourizing of the tissue in an animated video. See supporting information in the online version of this article.

made transparent, a 3D composition was created within AE that allowed flat 2D images to be manipulated within a 3D environment. In the 3D composition, all the images (now individual layers) occupied the same 3D space until layers were distributed evenly along the Z-axis. Unfortunately, AE does not provide a way to easily distribute multiple layers simultaneously along the Z-axis, therefore we used Layer Tools, a plug-in from Zaxwerks (Temple City, CA) to distribute the individual 2D images (or layers) evenly. Making all the individual layers subject to the control of a single layer called a 'null', allowed manipulation of the layers as a single 3D volume. The null layer was then animated to rotate the 3D object around all three axes. These animations are presented in the supplemental video files for Figs 1–3.

Results and discussion

High-resolution pixel-based images, which were captured with or without a microscope for different tissues, were imported into an interactive 3D environment using hardware and software commonly available in individual laboratories. Adobe After Effects is available for both PC and Mac, hence, either platform can be used. Because this technique uses popular commercially available software, all options available to the visual effects (VFX) community are available to the researcher. A combination of animation parameters such as rotation (in any axis), scaling, colour and lighting are available while viewing the 3D object and their use is limited only by the imagination of the researcher.

Features of Adobe After Effects used to reconstruct 3D images

Importing. Most pixel-based image formats can be imported into Adobe After Effects and used to build a 3D volume. We even imported obscure files such as OV2 files by renaming the extension of each image from '.ov2' to '.mov'. In Photoshop CS4 it is even possible to import DICOM images, then export them as TIFF or JPEG, which are easily imported into AE.

Registering. Alignment of individual serial images was the most tedious part of this procedure, but with a little practice we were able to align approximately 60 images per hour. Although auto alignment routines are available within AE, it was quicker and more accurate to manually align images as described earlier. Manual alignment also provides the researcher an opportunity to closely examine each 2D image individually.

Digital clearing. When a particular colour is removed (keyed-out), this allows the viewer to see through the image to structures underneath. This is directly analogous to chemical clearing of tissue to visualize features of interest. All images in a series can be digitally cleared simultaneously after importing them into AE as a sequence. In cases where one or two images reflect slightly different staining, it is also possible to clear

those images individually to enhance their consistency with the larger group.

Colour adjustment. The ability to make unwanted regions transparent (or to 'clear' them) and observe only structures of interest was based on differences in colours or differences in luminance after staining particular cellular attributes. Colour thresholds were chosen on the basis of visual observations of 2D images in which the borders of specific structures were identified. Because every colour in the various palates is assigned a specific number it was possible to precisely key-out the same colour in separate samples. Numerous colour correction routines within AE are available to adjust colours and allow clearing that at first appeared impossible because of colour similarity. This is illustrated in the woodchuck liver tissue (Fig. 2A), which was stained with eosin/haematoxylin (H&E; see 'Materials and methods') in various shades of red to purple. Some areas of the viable carcinoma/normal liver interface were too close in colour for the software to separate, so a mask (see below) was used to allow a form of contour tracing along the interface. However, using colour-correction routines in AE allowed adjustment of colours in original images to those shown (Fig. 2B); this kind of change allowed digital clearing of nearly any chosen structure or tissue.

Using a mask to highlight a specific feature. In cases where background tissue needed to be cleared but was the same colour as the structure of interest, a mask was generated to isolate part of the tissue. A mask can therefore be used to apply more than one colour clearing technique in the same image. The small bronchus of the lung (Fig. 3C) was isolated in this way. If the shape or size of the structure gradually changes over the series of images, the shape and size of the mask can be manually or automatically altered (using keyframes) to accommodate the change.

Computer-determined colours. Because the software precisely determines the selected colour (or luminosity) wherever it may appear in the image, researcher bias is minimized. Structures that may at first appear to be similar in colour (or luminance) may actually be different as determined by the software. In our research, structures sometimes became apparent after clearing that we had not noticed in the original 2D images because the software removed the colour of a particular channel (red, green or blue) 'leaving behind' structures that had been transformed into a different colour by the software.

Observations of tissue

Frozen oat plant. The crown (bottom 1–2 cm of the stem) (Fig. 1) of a winter cereal such as wheat (*Triticum aestivum*), barley, (*Hordeum vulgare*) rye (*Secale cereale*) or oat is the tissue from which a plant will re-grow if it survives winter. Two-dimensional histological observations of frozen oat plants have

been described in detail elsewhere (Livingston *et al.*, 2005, 2009).

Darkly staining regions in roots, within the crown of frozen plants and extending into some of the stems (Fig. 1B and D, Supporting Information) were never observed in unfrozen plants (not shown, see Livingston *et al.*, 2005) and are therefore assumed to be a freeze response. Because of their autofluorescence (unpublished observation) we have proposed (Livingston *et al.*, 2009) that these darkly stained regions are a result of the production of phenolic compounds similar to a disease response often seen in plants (Beckman, 2000). In the 3D volumes (Fig. 1D, Supporting Information) part of this darkly staining material formed what appeared to be a barrier in a general concave shape in the upper portion of the crown, bordering the transition zone (see description of crown regions in Livingston *et al.*, 2009). In 2D images from histological analysis of freeze damage done previously (Livingston *et al.*, 2005, 2009) we were not able to determine the 3D shape of this putative barrier. 3D volumes of several plants have been constructed from frozen oats (not shown) and the barrier in all conformed to this general shape. Subtending the barrier was tissue in which cell structure was significantly disrupted and filled with empty areas devoid of tissue (shown as orange in Fig. 1C); this region of the crown was presumed to be nonfunctional.

The 'necrotic region' in the centre of the oat crown (Fig. 1C) is actually composed of numerous regions within the dark-staining barrier in which tissue was separated either by ice or by necrosis. By inverting the matte-channel these 'empty' spaces were filled with a solid colour to show for the first time the continuity in 3D space of tissue separated by freezing. Note the vertical channels in the inset image in 1C. We suggest that these channels are regions where vascular bundles were positioned before freezing.

This reconstruction would not have been possible at this resolution using CT or MRI, nor would it have been possible to reconstruct the entire crown using CLSM without cutting the crown into several pieces and stitching numerous images together. Contour tracing in 180 individual images would have been tedious at best and would likely have overlooked subtle freezing effects such as regions inside roots and stems that were damaged by freezing (Fig. 1B).

Woodchuck liver. Images of serial tissue sections were photographed without a microscope using a consumer-grade digital camera (see 'Materials and methods'). The different components of the tissue—normal liver, viable hepatocellular carcinoma and the central necrotic areas (a result of radiofrequency ablation which kills tissue by heat—see 'Materials and methods') were readily evident (Fig. 2A). The colour scheme of the characteristic H&E staining pattern allowed easy recognition of various structures because they have the same hue as the original 2D images in a typical single H&E stained section. This made identification

of anatomical features, such as the interface of viable and necrotic tissue (Fig. 2B), vessels, bile ducts and connective tissue more straightforward than would be the case with CT or MRI imaging. Crisp delineation between the tumour and surrounding normal tissue, and between tumour and areas of necrosis was evident (Fig. 2B and C) albeit in this case it was mainly due to masking between the two tissues.

Using these tinctorial differences in the 3D volume, it was possible to isolate the volume and configuration of each of the main components of the tissue (Fig. 2D, Supporting Information). The extent and total volume of the necrosis following treatment was readily evident and the relationship with adjacent features such as large vascular structures could also be determined (Fig. 2). Because of the 3D reconstruction the relationship of the course of the vessels and the areas of necrosis were more easily identified than they would be using single 2D slices. In this application, the spatial relationship of the inhibition of necrosis due to the heat loss in flowing blood vessels of different caliber and blood velocity (arteries versus veins) could be evaluated (not shown) throughout the entire sectioned sample and could be done for the entire tumour if more sections were included. The final 3D volume of the entire mass and of the isolated portions of viable and necrotic tissue offers an accurate assessment of tissue changes in the entire volume of the studied tissue simultaneously (Fig. 2D, Supporting Information). This will allow us to investigate the full extent of areas of invasion and necrosis, giving a clearer view of the tissue response to therapy and the aggressiveness of the primary tumour.

Mouse lung. With 3D reconstruction, the lung had a distinctly light and spongy appearance (Fig. 3D, Supporting Information), reflective of the actual inflated lung. The course of large airways could be discerned readily, as could larger blood vessels due to the different tinctorial qualities of these tissues when stained with H&E (Fig. 3B). Perfusion fixation is ideal for this 3D application because the alveoli are distended and the configuration of the pulmonary interstitium, and its extent of thickening, as well as alveolar contents, such as inflammatory infiltrate or edema would be readily apparent (not shown). The colour scheme shown (Fig. 3B and C) allows for easy recognition of various structures because they have the same hue as the 2D images in an H&E stained section making identification of both large and small pulmonary anatomical features more straightforward than would be the case with CT or MRI imaging. In addition, various types of exudate or edema could be identified (not shown) and the two processes could be distinguished based on the staining qualities of each. Furthermore, the volume of lung affected by each of these processes can be assessed using this method. To our knowledge, it is not possible to distinguish different types of fluid (exudate or edema) using CT, MRI or another 3D reconstruction protocol.

Shortcomings

Even though the final image is viewed in three dimensions it is based on a series of pixel-based images, not vectors. AE therefore does not generate a true 3D object file that can be imported into commercially available 3D software and manipulated as a 3D object. However, it is possible to use the 'auto-trace' routine and generate a vector-based contour at the edge of structures from which the colour has been cleared. The resulting vector-based image can be exported in a format compatible with 3D software.

It is not possible to loft or extrude individual pixel-based images in true 3D space. For that reason individual images are flat and when viewed on edge (see Fig. 1D, Supporting Information, for Frozen Oat Plant) they appear to momentarily disappear. As long as a large number of images were used and were placed relatively close to each other, this did not interfere with the visualization.

Because the 3D volume is not based on vectors, a contiguous skin that covers the entire image could not be generated. However, we successfully used the software Strata Foto 3D (Santa Clara, UT) to photograph plants at different angles and generate a vector-based image for use as a skin (not shown). We have been able to import the 3D skin generated by Strata into AE using ZaxWerks 3D Invigorator (a plug-in) and insert our AE-generated 3D volume inside. The best workflow to produce a model compiled from more than 100 images is being developed in an extension of the research reported here.

Conclusions and future prospects

Despite living in a 3D world, researchers are often limited to 2D observations of experimental samples. Although 2D scientific observations are sometimes sufficient, 3D observations would often be preferred but are hindered by excessive opacity of tissues surrounding objects of interest. This report provides a proof of concept that 3D volumes can be built from 2D, pixel-based images using a desktop computer and off-the-shelf software. The technique cannot replace the use of noninvasive optical sectioning that confers a fourth temporal dimension to imaging by CLSC, MRI and PET/CT. However, this technique provides an inexpensive and relatively simple way to construct pixel-based 3D volumes by digitally clearing tissue, stacking the images and then viewing actual internal structures without tracing contours. The opportunity to use and interpret the tinctorial patterns arising from common histological reagents in a 3D context (e.g. H&E or Saffranin/Fast Green for animal and plant tissues, respectively and) on tissues too small to be viewed by MRI or PET/CT but too large to be viewed by CLSC is invaluable. The technique is ideally suited for *in situ* hybridization analysis to detect the presence of mRNA in an anatomical context (unpublished data).

The method described can be applied to images at any magnification and to any tissue from which serial sections

can be cut. For large tissues (Fig. 2), the use of a microscope is not required. Tissue about the size of a biopsy can be readily analysed spatially to reveal relationships between normal and diseased tissues that currently can only be estimated in two dimensions by review of individual slides. Many other possible applications can be envisioned, such as the evaluation of the actual shape and volume of distinct cellular populations such as tumours or inflammatory infiltrates. In the liver, it should be possible to determine the course of bile ducts or hepatic vessels in normal and diseased states. In the lung, the extent of inflammation filling alveoli and the volume of samples with altered alveolar configuration could also be shown.

In addition to generating 3D reconstructions from sections for light microscopy, serial monochrome images generated by CT, were cleared based on differences in luminance of objects of interest (not shown). 3D volumes from the resulting images were constructed suggesting that 3D reconstructions from other serial monochrome images such as those from MRI and electron microscopy are also possible.

It is hoped that popular motion graphic software companies such as Adobe will recognize the value of their software to the scientific community and begin to tailor routines as they did in providing the potential to import DICOM images into the 3D section of Photoshop CS4. Two improvements to AE that would make the procedure described here considerably more elegant would be including a way to easily distribute layers in the Z dimension (such as a slider) and enabling a pseudo-extrusion of pixel-based images into z-space, not as in the routine 'shatter' but as in 'build a new volume from layers' in the 3D section of Photoshop CS4.

References

- Angeles, G., Owens, S.A. & Ewers, F. (2004) Fluorescence Shell: a novel view of sclereid morphology with the confocal laser scanning microscope. *Microsc. Res. Tech.* **63**, 282–288.
- Badea, C.T., Drangova, M., Holdsworth, D.W. & Johnson, G.A. (2008) In vivo small-animal imaging using micro-ct and digital subtraction angiography. *Phys. Med. Biol.* **53**, R319–R350.
- Beckman, C.H. (2000) Phenolic-storing cells: keys to programmed cell death and periderm formation in wilt disease resistance in general defense responses in plants? *Physiol. Mol. Pl. Pathol.* **57**, 101–110.
- Beekman, T. & Engler, G. (1994) An easy technique for the clearing of histochemically stained plant tissue. *Plant Mol. Biol. Reporter* **12**, 37–42.
- Berleth, T. & Jurgens, G. (1993) The role of *monopteros* in organizing the basal body region of the *Arabidopsis* embryo. *Development* **118**, 575–587.
- Bihan, O.L., Bonnafous, P., Marak, L., *et al.* (2009) Cryo-electron tomography of nanoparticle transmigration into liposome. *J. Struct. Biol.* **168**, 419–425.
- Bobik, M., Ellisman, M.H., Rudy, B. & Martone, M.E. (2004) Potassium channel subunit Kv3.2 and the water channel aquaporin-4 are selectively localized to cerebellar pinneau. *Brain Res.* **1026**, 168–178.

- Chen, H., Hughes, D.D., Chan, T.A., Sedat, J.W. & Agard, D.A. (1996) IVE (Image Visualization Environment): a software platform for all three-dimensional microscopy applications. *J. Struct. Biol.* **116**, 56–60.
- Curley, S.A. (2001) Radiofrequency ablation of malignant liver tumors. *The Oncologist* **6**, 14–23.
- Harrison, F.W. & Anderson, M. (1974) The application of Herr's 41/2 clearing technique to zoological tissues. *Hydrobiologia* **46**, 177–180.
- Haug, J.T., Haug, C., Maas, A., Fayers, S.R., Trewin, N.H. & Waloszek, D. (2009) Simple 3D images from fossil and recent micromaterial using light microscopy. *J. Microsc.* **233**, 93–101.
- Hepler, P.K. & Gunning, B.E.S. (1998) Confocal Fluorescence microscopy of plant cells. *Protoplasma* **201**, 121–157.
- Hutzler, P., Fischbach, R., Heller, W., et al. (1998) Tissue localization of phenolic compounds in plants by confocal laser scanning microscopy. *J. Exp. Bot.* **49**, 953–965.
- Ferrando, M. & Spiess, W.E.L. (2000) Review: confocal scanning laser microscopy. A powerful tool in food science. *Food Sci. Tech. Int.* **6**, 267–284.
- Kaeb, S. & Landthaler, M. (2009) Confocal laser scanning microscopy – evaluation of native tissue sections in micrographic surgery. *Lasers Med. Sci.* **24**, 819–823.
- Kremer, J.R., Mastronarde, D.N. & McIntosh, J.R. 1996. Computer Visualization of three-dimensional image data using IMOD. *J. Struct. Biol.* **116**, 71–76.
- Kriete, A. & Schwebel, T. (1996) 3-D TOP – a software package for the topological analysis of image sequences. *J. Struct. Biol.* **116**, 150–154.
- Livingston, D.P., III, Tallury, S.P., Premakumar, R., Owens, S.A. & Olien, C.R. (2005) Changes in the histology of cold hardened oat crowns during recovery from freezing. *Crop. Sci.* **45**, 1545–1558.
- Livingston, D.P., III, Tuong, T.D., Haigler, C.A., Avci, U. & Tallury, S.P. (2009) Rapid microwave tissue processing of winter cereals for histology allows identification of separate zones of freezing injury in the crown. *Crop. Sci.* **49**, 1837–1842.
- Liedl, B.E., McCormick, S., & Mutschler, M.A. (1993) A clearing technique for histochemical location of GUS activity in pollen tubes and ovules of *Lycopersicon*. *Plant Mol. Biol. Reporter* **11**, 194–201.
- Lux, A., Morita, S., Abe, J. & Ito, K. (2005) An improved method for clearing and staining free-hand sections and whole mount samples. *Ann. Bot.* **96**, 989–996.
- Marko, M., Leith, A. (1996) Three-dimensional reconstruction from stereoscopic contouring. *J. Struct. Biol.* **116**, 93–98.
- Patriciu, A., Awad, M., Solomon, S.B., Choti, M., Mazilu, D., Kavoussi, L. & Stoianovici, D. (2005) Robotic assisted radio-frequency ablation of liver tumors – randomized patient study. *Med. Image Comput. Comp.-Assist. Interv.* **3750**, 526–533.
- Peyrin, F. (2009) Investigation of bone with synchrotron radiation imaging: from micro to nano. *Osteoporos Int.* **20**, 1057–1063.
- Saueremann, K., Gambichler, T., Jaspers, S., et al. (2002). Histometric data obtained by in vivo confocal laser scanning microscopy in patients with systemic sclerosis. *BMC Dermatol.* **2**, 8–14.
- Shotton, D.M. (1989) Confocal scanning optical microscopy and its applications for biological specimens. *J. Cell Sci.* **94**, 175–206.
- Sun, M.G., Williams, J., Munoz-Pinedo, C., Perkins, G.A., Brown, J.M., Ellisman, M.H., Green, D.R. & Frey, T.G. (2007) Correlated three-dimensional light and electron microscopy reveals transformation of mitochondria during apoptosis. *Nat. Cell Biol.* **9**, 1057–1065.
- Zimmerman, A. (1893) Botanical Microtechnique. Translated from German by Humphrey, J.E. Henry Holt and Co., New York. P8–18. Entire book has been put on-line by Google at the following link: <http://books.google.com/books?id=9qgUAAAAAYAAJ&ots=1w-oUdxDUL&dq=botanical%20microtechnique%20Zimmerman&pg=PR1> After reaching the site click on the button entitled “read book”. Alternatively, one is also able to download a pdf version of the complete book.

Supporting Information

Additional Supporting Information may be found in the online version of this article:

- Supplementary video for Fig. 1.
- Supplementary video for Fig. 2.
- Supplementary video for Fig. 3.

Please note: Wiley-Blackwell are not responsible for the content or functionality of any supporting materials supplied by the authors. Any queries (other than missing material) should be directed to the corresponding author for the article.